Detection of gamma-ray halos
around nearby late-type galaxies

M. S. Pshirkov*

Sternberg Astronomical Institute,
Lomonosov Moscow State University,
Universitetsky prospekt 13, 119992, Moscow, Russia

Institute for Nuclear Research of Russian Academy of Sciences,
60th October Anniversary Prospect,
7a, 117312, Moscow, Russia
and
Lebedev Physical Institute, Astro Space Center, Pushchino Radio Astronomy Observatory 142290,
Radioteleskopnaya 1a, Moscow reg., Pushchino, Russia

B. A. Nizamov†

Sternberg Astronomical Institute,
Lomonosov Moscow State University,
Universitetsky prospekt 13, 119992, Moscow, Russia

(Dated: October 4, 2024)

Various theoretical models predict existence of extended γ-ray halo around normal galaxies, that could be produced by interactions of cosmic rays with the circumgalactic medium or by annihilation or decay of hypothetical dark matter particles. Observations of the closest massive galaxy M31 also corroborate this possibility. In this study we search for gamma-ray emission from the galaxies within 15 Mpc at energies higher than 2 GeV and try to assess its spatial extension. We use the latest catalog of local galaxies and apply a simple yet robust method of aperture photometry. By imposing the mass, energy, and spatial cuts, we selected a set of 16 late-type galaxies and found a statistically significant excess above the background level ($p - \mathrm{val} = 4.8 \times 10^{-9}$). More importantly, our analysis shows that this excess can be ascribed to an extended source with a radius $\sim 0.3°$ rather than a point-like one. In contrast, 6 early-type galaxies, which satisfied the same cuts, showed no excess. Our results are supported by the stacking likelihood analysis technique. The difference between the late- and early-type galaxies and a rather irregular shape of the extended source that we found indicate that this high-energy emission is not due to DM annihilation/decay but rather originates from cosmic ray interaction with the circumgalactic medium.

I. INTRODUCTION

At the present level of the instrument sensitivity high-energy γ-ray sky ($E > 100$ MeV) is dominated by the active galactic nuclei (AGNs) of various types: there are 4008 AGNs out of the 7194 sources total in the latest catalog of the Fermi LAT sources [1]. Much more modest contribution comes from star forming galaxies, due to their lower intrinsic luminosities, especially for normal galaxies without ongoing bursts of star-formation. Only a handful of these galaxies have been detected [2–4] as individual sources, although by some estimations their whole population could be a major contributor to the extragalactic diffuse γ-ray background [5]. The γ-ray emission in star-forming galaxies mostly originates in collisions of galactic cosmic rays (CRs) with interstellar galactic medium – the same process that produces the diffuse γ-raygalactic background in the Milky Way. Also a considerable fraction of emission comes from

the galactic sources: pulsars, PWNe, etc. This emission is largely confined to the extension of the galaxy, $\mathcal{O}(10 \text{ kpc})$. Due to the limited angular resolution of the instruments, around $1°$ at GeV energies, almost all detected galaxies are best described as point sources. Spatially extended emission was detected around two normal galaxies: first, detection of famous Fermi bubbles [6, 7] –large, $\mathcal{O}(10 \text{ kpc})$ lobes above and below the Galactic center; second, there is growing certainty that the M31 galaxy is also surrounded by an extended γ-ray halo [8, 9]. Extended emission could arise from previous phases of AGNs activity, similarly to the cases of the γ-ray lobes of the Cen A and Fornax A galaxies [10, 11], or it could be produced by the population of the galactic CRs gradually leaking into the circumgalactic medium and accumulating there on time scales of Gyrs [12, 13]. Alternatively, γ-ray halo could emerge from processes of annihilation or decay of dark matter (DM) particles [14]. Both observations of M31 and models predict for MW-like galaxies γ-ray luminosity in $10^{38} - 10^{39}$ erg s^{-1} range.

As individual sources are expected to be weak and lie below the detection threshold, we analyzed aggregated observations of nearby massive galaxies and stacked

* pshirkov@sai.msu.ru
† nizamov@physics.msu.ru

sources in order to increase our sensitivity. In this *Letter* we report a discovery of a statistically significant ($p-$val $= 4.8 \times 10^{-9}$) excess of photons at energies > 2 GeV around local ($D < 15$ Mpc) massive late-type galaxies. Observations at higher energies, where the *Fermi* LAT angular resolution is considerably better, allowed to show that the excess is extended with $\sim 0.3°$ radial size.

II.   DATA AND METHODS

For our analysis we used the photon database of *Fermi* LAT [15]. We selected photons belonging to the *SOURCE* class, reconstruction version PASS8R3 with energies $E > 1$ GeV and zenith angle $\theta < 105°$ in order to avoid contamination from the Earth's limb. Observations span the time interval from 04 Aug 2008 (MET=239557417) to 09 Aug 2024 (MET=744865715). For an analysis with Fermi science tools (version 2.2.0) we adopted standard quality cuts. We utilized one of the latest catalogs of nearby galaxies by Ohlson et al. [16]. There are mass, distance, and morphological type estimations for 15424 galaxies closer than 50 Mpc. Our target set was constructed using several cuts: on the galaxy mass, its distance and its sky position with regard to *Fermi* sources. First, we estimated the distance threshold, demanding that the observed number of photons in 16 years of the observations for a source with a luminosity $L(> 1$ GeV$) \sim 5 \times 10^{38}$ erg s^{-1} was larger than 10. That gave an upper limit on a distance, $D_{max} = 15$ Mpc. The lower limit comes from a requirement that the sought halo, which has a radius in 50–100 kpc range, should not be too extended, that is larger than $1°$, because such a weak extended object would be extremely difficult to detect ($D_{min} = 5$ Mpc). The mass threshold was set at $M_* = 10^{10} \ M_\odot$, where M_* is the stellar mass. Ohlson et al. derived the stellar masses from the color – mass-to-light ratio from [17] where $g - i$ photometry is available, and they extended this ratio to other colors using galaxies for which a $g - i$ color is available along with some other color $[(g - r)_0, (B - V)_0, (B - R)_0]$. Adoption of mass and distance cuts reduced the number of sources to 87. Adoption of a higher threshold, e.g. $10^{10.5} M_\odot$, would result in a much smaller number of available targets. A lower threshold would lead to a great decrease in expected signal, if it was produced in CR-related models, but not so much in DM-related models. Therefore, we reserved the $10^9 - 10^{10} \ M_\odot$ mass range to check the hypothesis that the detected signal had been produced by annihilation or decay of DM particles.

We exploited a simple statistical method similar to aperture photometry: we compared the number of photons observed within the radius R from the source (we call this circle the ON-region) with the number of photons expected in this region in absence of any source. The latter was calculated from the number of photons observed in the OFF-region which was the annulus with the inner and outer radia of R and $2R$, respectively. The smallest angular scale that can be effectively probed with that method corresponds to $R = PSF_{68}$, i.e. the 68% containment angle of the point-spread function, which depends on the energy and the conversion type.

As the expected level of signal was low, we needed to select galaxy targets far from possible interfering sources and regions with high background. Thus, we imposed a latitude cut, removing all low-latitude galaxies with $|b| < 20°$. Even a weak close γ-ray source could lead to a spurious detection or overestimation of the background in the OFF-region, which in turn would greatly diminish the sensitivity of our method. Hence, we removed from the sample all the galaxies with a neighboring 4FGL-DR4 source closer than $3PSF_{68}$. Finally, we set a threshold energy E_0: on the one hand, we would like to have it as low as possible for the sake of increase of photon statistics; on the other, PSF size quickly increases for lower energies, making our last cut prohibitively restricting. We chose $E_0 = 2$ GeV, $PSF_{68}(E_0)$=0.5°; after implementing latitude and 4FGL-proximity cuts we were left with 22 sources out of 87 initial sources that satisfied both mass and distance conditions. For lower threshold $E_0 = 1$ GeV with correspondingly wider PSF, the 4FGL-proximity cut becomes too effective, leaving no candidate sources.

For our selected threshold, $R = 0.5°$, there are 1890 events in 22 ON-regions, while the expected number estimated from the OFF-regions is 1719 events, and the corresponding $p-$val $= 2.7 \times 10^{-5}$. However, if we split our set into subsets of early-type (6 galaxies) and late-type galaxies (16 galaxies) a striking difference emerges: for the former subset, there is a *deficit* of events, 500 observed vs. 533 expected, while in the latter one the excess becomes much more statistically significant, 1390 observed vs. 1186 expected, $p -$val $= 4.8 \times 10^{-9}$. From that moment we focused on this subset, which is shown in Table I.

We repeated our analysis for different energy cuts and different conversion types – front+back and front only for an increased angular resolution (See Table II). Our results are presented in the Table III.

The maximal signal was achieved for front-converted photons with $E_0 = 3$ GeV and $R = 1.5PSF_{68}(3$ GeV$) = 0.375°$: 263 observed photons vs. 171 expected photons, $p -$val $= 6.0 \times 10^{-11}$. Also our estimates of the probability are conservative at the lower energies, 2 and 3 GeV (front+back conversions), where $R \sim PSF_{68}$. In our approach we assumed that all the excess photons were contained inside R, and the OFF-regions were free from them. However, it is certainly not the case at lower energies with $R \sim PSF_{68}$, where almost a third of the excess photons would spill over into the OFF-regions, artificially increasing the background estimates and diluting the statistical significance of a detection. Correcting for the spill-over effect, we would expect ~ 1150 and 320 instead of 1186 and 335 events for energies 2 and 3 GeV correspondingly, and that would greatly decrease

the probabilities, to $\sim 10^{-11}$ and $\sim 10^{-10}$ levels. However, for the sake of consistency, we do not quote these values in the Table III.

III. RESULTS AND DISCUSSION

Could our detected excess arise due to some flaw in our adopted approach? Although we did not observe any excess signal around six early-type galaxies, some additional observations with larger number of targets were needed to settle the issue. We repeated our analysis in the neighbouring mass bin $10^9 \ M_\odot < M < 10^{10} \ M_\odot$. There are 199 galaxies in 5-15 Mpc distance range, after imposing spatial cuts we were left with 44 galaxies satisfying our conditions, 12 early- and 32 late-type galaxies. No significant excess was detected: 3697 observed photons, when 3700 were expected for total selection and 2618 vs. 2686 for the late-type subset.

We can conclude that the possible DM-related contribution is not the major cause of the excess observed for $M > 10^{10} \ M_\odot$ late-type galaxies. First, in that case we would observe such signal for early-type high-mass galaxies as well. Second, we would expect considerable signal from the lower-mass set: in this mass range there is only weak dependence of the expected halo mass on the stellar mass (e.g. [18]): decrease in the stellar mass from 10^{10} to $10^9 \ M_\odot$ leads only to corresponding decrease of 0.4 dex in the mass of the halo. In this narrow mass range we could roughly expect linear dependence of DM-related signal on the mass of the halo, so from our results for $E_0 = 2$ GeV and $R = PSF_{68}$ we would expect the excess signal around 32 late-type galaxies of around 150 events, instead of ~ 70 photons deficit that we actually observe.

Could our cut on neighbouring *Fermi* sources (further than $3PSF_{68}(2 \text{ GeV}) = 1.5°$) be too mild and the observed excess be just a pollution from strong nearby sources, that by chance occurred to reside near our targets? We performed our analysis for several directions at a distance of 1.5 degree (3 PSF at 2 GeV) from the strongest high-latitude ($|b| > 20°$) source, PSR J1836+5925 (4FGL J1836.2+5925). Instead of excess events we found strong deficit, ~ 310 observed vs ~ 480 expected. We can safely state that with our adopted cuts strong sources can only boost the number of events in OFF-regions and consequently give rise to apparent *deficit* in the central regions. Additionally, we have checked that even a very strong source at 1.5 degrees distance does not affect our estimates of the background at energies higher than 2 GeV because of the rapidly shrinking PSF size.

A. Morphology

Our results show that the excess was not produced by the point-like sources, like low-luminosity AGNs in the centers of galaxies or galaxies themselves. If it was the
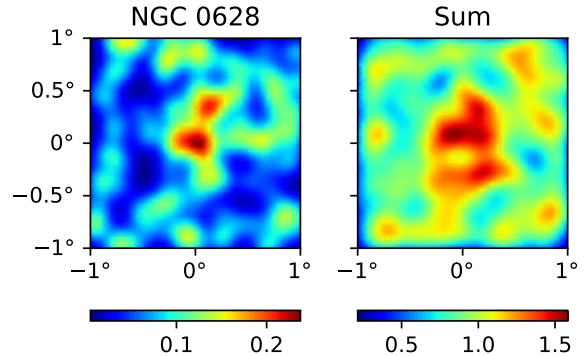

FIG. 1. Count maps of NGC 0628 *(left)* and of the sum of all 16 sources *(right)* using front-converted photons above 3 GeV. The maps are smoothed using a Gaussian kernel with $\sigma = 0.1°$. Coordinates are given with respect to the map center.

case, the maximal significance at different energies would be achieved at angular scales corresponding to PSF size at these energies and it is manifestly not so (see Table III). The angular size, corresponding to the maximal signal, changes with increasing angular resolution: from $\sim 0.5°$ at 2 GeV to $\sim 0.3°$ at 3 GeV. However, it does not decrease further up to the energies as high as 10 GeV, where the angular resolution is twice as high (Table II). These results are consistent with a spatial excess around $0.3°$ size, which, for $D = 15$ Mpc corresponds to $r_h = 80$ kpc.

At energies higher than 3 GeV for front converted photons we constructed joint count map from the count maps of 16 individual sources (see Fig. 1) The excess is clearly seen and has an irregular shape: this fact disfavors a simple model of a smooth halo, like one of decaying DM or quasi-uniform halo of CRs interacting with the CGM. Instead it looks like a superposition of weaker substructures from the individual sources: as an illustration we show in the same figure the count map of the strongest individual source, NGC 0628 – there is a hint on some sort of lobes protruding from the central part of the galaxy.

B. Likelihood analysis and test statistics

We also analyzed our set, using standard Fermi Science tools [19], such as *gtlike* which employs the maximum likelihood approach [20]. Even the most prominent candidate, NGC 0628 was detected at 2 GeV only at the test statistic TS ~ 6 level ($\sim 2.4\sigma$) when we included it as a point source in our source model. Comparable level of detection was achieved with an extended uniform disk templates with a radius in a 0.2-$0.4°$ range, although as it is evident from Fig. 1 such a simple template could not effectively reproduce actual pattern of emission. At

the highest energies, $E > 10$ GeV point source model fared worse, giving TS ~ 2 and a *decrease* in total likelihood, $\Delta LLH = -0.6$, while an extended uniform 0.3 degree disk model provided a slight *increase*, $\Delta LLH = 2.4$. These values are marginally significant, only hinting on a prevalence of an extended template. We performed stacking analysis using the code FERMI_STACKING[21] which has been previously applied in different studies, e.g., in a search for dark matter annihilation in the Milky Way dwarf spheroidal galaxies [22]. The pipeline is described in [23]: for each individual source, the code assigns it a flux value and a spectral index value from the given intervals and computes its TS for every combination of these values. This gives a 2D-array of TS values. Such arrays for all the sources in study are then added to produce the final TS array such as the one shown in Fig. 3. The flux and index values corresponding to the global maximum can be regarded as average values for the sample in study. We performed the stacking analysis for several E_0 and, by a slight modification of the code, for a point and extended test source (for the latter, the RadialDisk model was used with the radius of $0.3°$). The code also makes a so-called evolution plot which shows the maximum stacked TS vs. the number of sources in the stack. The plot for the analysis with $E_0 = 2$ GeV is shown in Fig. 2. The lower x-axis and the red solid line correspond to stacking of point sources, while the upper x-axis and the blue dashed line correspond to stacking of extended sources. The sources on each axis are sorted in descending order of individual TS's. For example, in the point source analysis, the source NGC 7331 has the
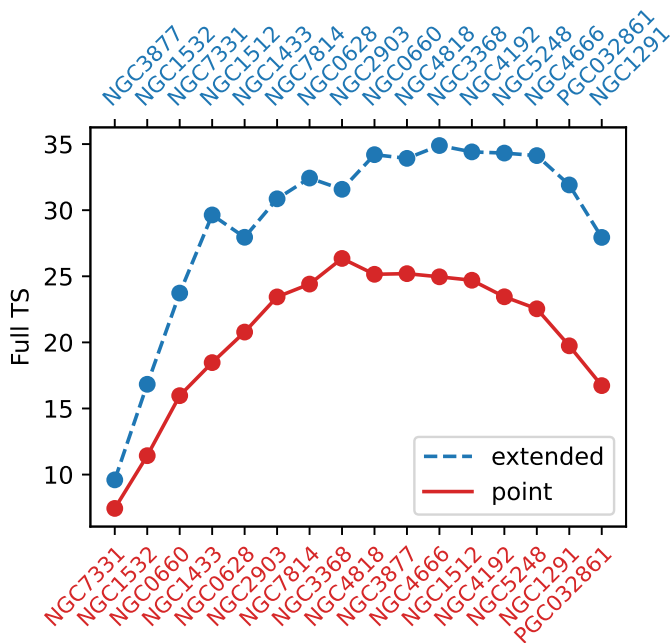
largest individual TS, and the first red point corresponds to the stack consisting of NGC 7331 only. The second-largest TS is obtained for NGC 1532, and the second red point corresponds to a stack consisting of NGC 7331 and NGC 1532, and so on. Note that the positions of maxima in individual TS arrays can be different from the position of the global maximum. In fact, an individual TS for some source at the position of the global maximum can be negative which is why the evolution plots have a decreasing part. Note also that the individual TS-ranking is not the same in the point and extended source analysis. For example, NGC 7331 has the largest TS in the point source analysis, but only the third-largest one in the extended source analysis. From Fig. 2 it is evident that the extended stacked source achieves considerably larger TS value than the point source. In Fig. 3, we show the stacked TS array for extended source analysis where only sources with positive contributions to the global TS are added to the stack. The maximum global TS is 36, the best flux is $3.67^{+0.98}_{-1.38} \times 10^{-11}$ phot cm^{-2} s^{-1}, and the best index is $2.8^{+0.6}_{-0.4}$.

There are also quite clear drawbacks of this approach – as the fluxes of all sources are identical and fixed, for a weaker source it would lead to a worse fit and accordingly to decrease in the aggregate TS. However, almost all these weaker sources give coherent positive contribution to the statistical significance in our ON-OFF approach and are detected there as well, albeit with a lower significance. We split our set into two subsets, each com-

FIG. 2. Evolution plots for the point *(red solid)* and extended *(blue dashed)* source analyses with $E_0 = 2$ GeV.
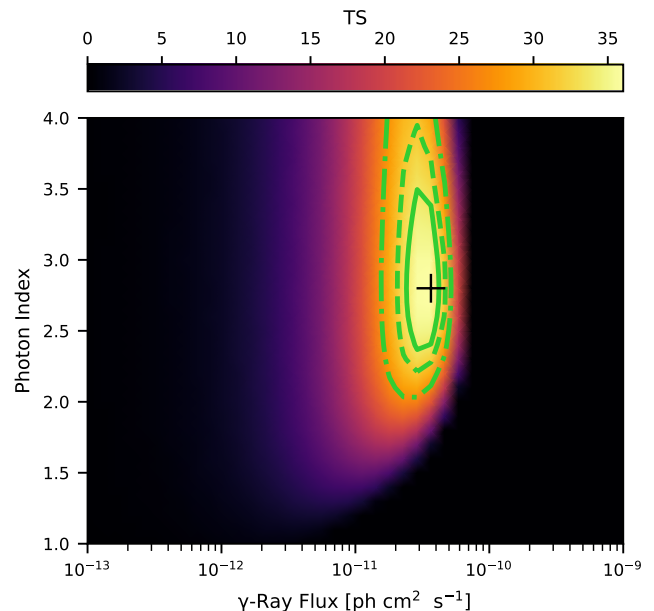

FIG. 3. Stacked TS array for the eight sources which provide positive contributions to the full TS in the extended source analysis with $E_0 = 2$ GeV. Green lines denote the levels of significance of 1, 2 and 3σ. The black cross shows the position of the TS maximum.

prising eight sources. In the first one we included sources giving considerable positive TS contribution (NGC0628, NGC0660, NGC1512, NGC1532, NGC3368, NGC3877, NGC7331, NGC7814) and the other comprised the rest (NGC1291, NGC1433, NGC2903, NGC4192, NGC4666, NGC4818, NGC5248, PGC032861). Not surprisingly, the first subset performed much better at 2 GeV (785 observed vs 625 expected, $p-$val $= 4.1 \times 10^{-10}$) comparing to the second one (605 vs 562, $p-$val $= 3.6 \times 10^{-2}$). However, the situation is different at higher energies, e.g. at 5 GeV the contributions are roughly equal (126/91, $p-$val $= 3.0 \times 10^{-4}$ and 112/78, $p-$val $= 1.4 \times 10^{-4}$). This behaviour shows that the properties of our sources are far from being identical – they have different luminosities and different spectral indices, and the subset of the weaker sources demonstrates a much harder spectrum. It is obvious that this spread in the properties of individual sources and impossibility to sufficiently describe their shapes with one simple identical template would lead stacking approach we used to underestimate the true statistical significance of detection of the extended emission.

FIG. 4. Spectra of the full (16 galaxies) sample, 'strong' and 'weak' subsamples.

C. Spectrum and power

We could not easily obtain mean luminosity and characteristic spectral index of the sources due to an obvious heterogeneity of our set. Instead of that, we analyzed separately two subsamples ('weak' and 'strong') defined above. We estimated indices and luminosity very roughly, using the number counts of excess photons and assuming that the excess had a characteristic 0.3 degree size. Results for the full set and both subsets are presented in Figs. 4, 5: it can be seen that the galaxies in the 'weak' subset have much harder spectrum, $\alpha_{\text{weak}} \sim 1.7$, than their counterparts in the 'strong' subset, $\alpha_{\text{strong}} \sim 2.7$. Both values should be taken as crude estimates only: the aperture photometry approach has rather limited accuracy for this task and even after dividing the set into 'weak' and 'strong' parts the resulting subsets are not very homogenous. Encouragingly, the analysis with FERMI_STACKING gives very close values of spectral indices: $2.8^{+0.6}_{-0.4}$ and $1.7^{+1.1}_{-0.5}$ for the 'strong' and 'weak' subsets respectively. Estimates of average luminosities are not too different for galaxies in both subsamples, $L_{\text{strong}} \sim 5.6 \times 10^{39}$ erg s^{-1} and $L_{\text{weak}} \sim 2.3 \times 10^{39}$ erg s^{-1} for adopted distance $D = 15$ Mpc and total *Fermi* LAT exposure $\mathcal{E} = 8 \times 10^{11}$ cm^2 s. Absence of signal at $E = 30$ GeV implies that the spectra demonstrate a cut-off or at least considerable softening at energies $E > 10$ GeV. We are going to investigate the difference between the two subsets more thoroughly elsewhere.
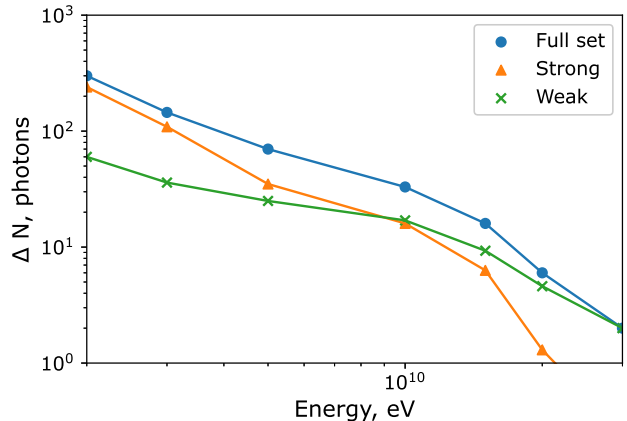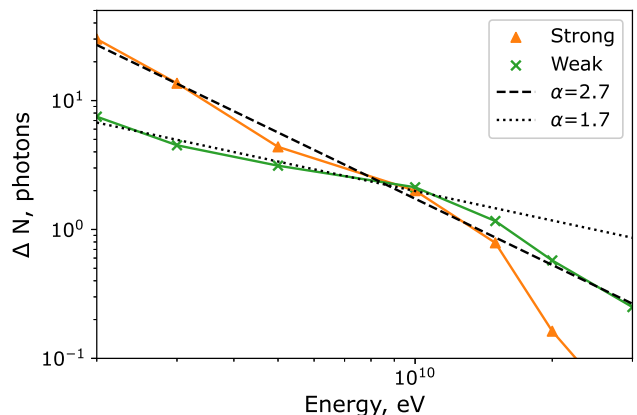

FIG. 5. Mean spectra of 'individual' galaxies, reduced from Fig. 4 using number of galaxies in relevant subsamples. Best power-law fits for the energy range (2-10) GeV are presented. Cut-offs at higher energies are clearly seen for both subsamples.

IV. CONCLUSIONS

In this paper, we searched for γ-ray signal from nearby galaxies ($D < 15$ Mpc) using a method of aperture photometry. We extracted a sample of galaxies with stellar masses larger than 10^{10} $M_{\odot}$ from up-to-date catalog [16] and selected all the sources with galactic latitudes $|b| > 20°$ residing further than $1.5°$ from γ-ray sources from *Fermi* -LAT 4FGL-DR4 catalog. We detected a statistically significant signal at energies higher than 2 GeV from the set of 16 late-type galaxies, $p-$val $\sim 4.8 \times 10^{-9}$. The highest significance was achieved for front-converted events with $E > 3$ GeV: $p -$ val $\sim 6 \times 10^{-11}$. Analysis at different energies showed that the excess is spatially extended, with an angular size $\sim 0.3°$, corresponding to a linear size around 80 kpc. The γ-ray properties of se-

lected late-type galaxies are not identical: half of galaxies have higher average luminosity and demonstrate soft spectrum with spectral index $\alpha \sim 2.7$, while the rest are less luminous and have much harder spectrum, $\alpha \sim 1.7$

The γ-ray emission from star forming galaxies can contribute to the isotropic γ-ray background as suggested in [13]. The authors found that the gaseous halo around the Milky Way can emit $\sim 10^{39}$ erg/s above 100 MeV. If such a luminosity is scaled with the galactic stellar mass, it can contribute a few per cent of the γ-ray background. The luminosity we found in this work is more than an order of magnitude larger than the estimate in [13] (the galaxies in study have stellar masses comparable to that of the Milky Way), thus we could expect that halos may contribute up to several tens per cent of the background.

ACKNOWLEDGMENTS

Appendix: Tables

In Table I we show the sample of late-type galaxies where the extended gamma-ray halos were discovered.

In Table II PSF values are shown for the relevant photon energies.

In Table III the results of the aperture photometry analysis are summarized.

TABLE I. Galaxies used as targets in our analysis. Properties are taken from [16]

#	Name	$l,°$	$b,°$	D, Mpc	$\log M/M_\odot$
1	NGC0628	138.617	-45.705	10.19	10.128 ± 0.136
2	NGC0660	141.607	-47.347	11.57	10.098 ± 0.331
3	NGC1291	247.524	-57.042	9.08	10.707 ± 0.136
4	NGC1433	255.691	-51.195	9.04	10.070 ± 0.201
5	NGC1512	248.668	-48.166	11.63	10.172 ± 0.160
6	NGC1532	233.168	-46.584	14.26	10.528 ± 0.600
7	NGC2903	208.710	44.540	8.87	10.404 ± 0.136
8	NGC3368	234.435	57.010	10.42	10.523 ± 0.136
9	NGC3877	150.719	65.956	14.63	10.096 ± 0.476
10	NGC4192	265.434	74.960	12.68	10.371 ± 0.136
11	NGC4666	299.538	62.368	14.70	10.298 ± 0.136
12	NGC4818	305.212	54.323	11.04	10.008 ± 0.530
13	NGC5248	335.929	68.751	13.75	10.264 ± 0.606
14	NGC7331	93.722	-20.724	12.62	10.724 ± 0.327
15	NGC7814	106.410	-45.175	14.40	10.520 ± 0.136
16	PGC032861	245.103	55.513	14.45	12.827 ± 0.502

[1] J. Ballet, P. Bruel, T. H. Burnett, B. Lott, and The Fermi-LAT collaboration, Fermi Large Area Telescope Fourth Source Catalog Data Release 4 (4FGL-DR4), arXiv e-prints , arXiv:2307.12546 (2023), arXiv:2307.12546 [astro-ph.HE].

[2] M. Ackermann et al., GeV Observations of Star-forming Galaxies with the Fermi Large Area Telescope, ApJ 755, 164 (2012), arXiv:1206.1346 [astro-ph.HE].

[3] M. Ajello, M. Di Mauro, V. S. Paliya, and S. Garrappa, The γ-Ray Emission of Star-forming Galaxies, ApJ 894, 88 (2020), arXiv:2003.05493 [astro-ph.GA].

[4] A. Ambrosone, M. Chianese, and A. Marinelli, Constraining the hadronic properties of star-forming galaxies above 1 GeV with 15-years Fermi-LAT data, J. Cosmology Astropart. Phys. 2024, 040 (2024), arXiv:2402.18638 [astro-ph.HE].

[5] M. A. Roth, M. R. Krumholz, R. M. Crocker, and S. Celli, The diffuse γ-ray background is dominated by star-forming galaxies, Nature 597, 341 (2021), arXiv:2109.07598 [astro-ph.HE].

[6] M. Su, T. R. Slatyer, and D. P. Finkbeiner, Giant Gamma-ray Bubbles from Fermi-LAT: Active Galactic Nucleus Activity or Bipolar Galactic Wind?, ApJ 724, 1044 (2010), arXiv:1005.5480 [astro-ph.HE].

[7] M. Ackermann et al., The Spectrum and Morphology of the Fermi Bubbles, ApJ 793, 64 (2014), arXiv:1407.7905 [astro-ph.HE].

[8] M. S. Pshirkov, V. V. Vasiliev, and K. A. Postnov, Evidence of Fermi bubbles around M31, MNRAS 459, L76 (2016), arXiv:1603.07245 [astro-ph.HE].

[9] C. M. Karwin, S. Murgia, S. Campbell, and I. V. Moskalenko, Fermi-LAT Observations of γ-Ray Emission toward the Outer Halo of M31, ApJ 880, 95 (2019), arXiv:1812.02958 [astro-ph.HE].

[10] R. Z. Yang, N. Sahakyan, E. de Ona Wilhelmi, F. Aharonian, and F. Rieger, Deep observation of the giant radio lobes of Centaurus A with the Fermi Large Area Telescope, A&A 542, A19 (2012).

[11] M. Ackermann et al. (Fermi LAT Collaboration), Fermi

TABLE II. Values of the 68% containment angle of the point-spread function (PSF$_{68}$) for different energies and conversion types – front and front+back.

Energies	PSF$_{68}$, °
2 GeV	0.50
2 GeV front	0.34
3 GeV	0.36
3 GeV front	0.25
5 GeV	0.25
5 GeV front	0.17
10 GeV	0.17
30 GeV	0.11

TABLE III. Results of our analysis for different energy thresholds, conversion types and radii of the ON-region R. In each cell, the two numbers divided by a slash are, respectively, the observed and expected numbers of events for a given selection of E_0, conversion type, and R, followed by the corresponding p-val, assuming a Poissonian distribution for the background. Table cells with text in bold correspond to $R = PSF_{68}(E, \text{conversion type})$.

	$\sim 0.25°$	$\sim 0.35°$	$\sim 0.5°$
2 GeV	-	$723/588\ 4.2 \times 10^{-8}$	$\mathbf{1390/1186,\ 4.8 \times 10^{-9}}$
2 GeV front	-	$\mathbf{355/280,\ 9.2 \times 10^{-6}}$	$750/605,\ 7.8 \times 10^{-9}$
3 GeV	-	$\mathbf{441/335,\ 2.1 \times 10^{-8}}$	$912/767,\ 2.0 \times 10^{-7}$
3 GeV front	$\mathbf{102/91,\ 0.16}$	$263/171,\ 6.0 \times 10^{-11}$	$430/322,\ 8.2 \times 10^{-9}$
5 GeV	$\mathbf{102/92,\ 0.16}$	$238/168,\ 2.8 \times 10^{-7}$	$378/318,\ 6.2 \times 10^{-4}$
5 GeV front	$63/52,\ 0.07$	$112/70,\ 2.3 \times 10^{-6}$	$221/170,\ 1.0 \times 10^{-4}$
10 GeV	$43/34,\ 0.09$	$80/47,\ 9.4 \times 10^{-6}$	$147/122,\ 0.26$
30 GeV	-	$12/12,\ 0.53$	$36/32,\ 0.016$

Large Area Telescope Detection of Extended Gamma-Ray Emission from the Radio Galaxy Fornax A, ApJ **826**, 1 (2016), arXiv:1606.04905 [astro-ph.HE].

[12] R. M. Crocker and F. Aharonian, Fermi Bubbles: Giant, Multibillion-Year-Old Reservoirs of Galactic Center Cosmic Rays, Phys. Rev. Lett. **106**, 101102 (2011), arXiv:1008.2658 [astro-ph.GA].

[13] R. Feldmann, D. Hooper, and N. Y. Gnedin, Circumgalactic Gas and the Isotropic Gamma-Ray Background, ApJ **763**, 21 (2013), arXiv:1205.0249 [astro-ph.HE].

[14] T. Bringmann and C. Weniger, Gamma ray signals from dark matter: Concepts, status and prospects, Physics of the Dark Universe **1**, 194 (2012), arXiv:1208.5481 [hep-ph].

[15] W. B. Atwood *et al.*, The Large Area Telescope on the Fermi Gamma-Ray Space Telescope Mission, ApJ **697**, 1071 (2009), arXiv:0902.1089 [astro-ph.IM].

[16] D. Ohlson, A. C. Seth, E. Gallo, V. F. Baldassare, and J. E. Greene, The 50 Mpc Galaxy Catalog (50 MGC): Consistent and Homogeneous Masses, Distances, Colors, and Morphologies, AJ **167**, 31 (2024), arXiv:2309.05701 [astro-ph.GA].

[17] E. N. Taylor *et al.*, Galaxy And Mass Assembly (GAMA): stellar mass estimates, MNRAS **418**, 1587 (2011), arXiv:1108.0635 [astro-ph.CO].

[18] F. Shankar, A. Lapi, P. Salucci, G. De Zotti, and L. Danese, New Relationships between Galaxy Properties and Host Halo Mass, and the Role of Feedbacks in Galaxy Formation, ApJ **643**, 14 (2006), arXiv:astro-ph/0601577 [astro-ph].

[19] Https://github.com/fermi-lat.

[20] J. R. Mattox *et al.*, The Likelihood Analysis of EGRET Data, ApJ **461**, 396 (1996).

[21] https://fermi-stacking-analysis.readthedocs.io/en/latest/.

[22] A. McDaniel, M. Ajello, C. M. Karwin, M. Di Mauro, A. Drlica-Wagner, and M. A. Sánchez-Conde, Legacy analysis of dark matter annihilation from the Milky Way dwarf spheroidal galaxies with 14 years of Fermi -LAT data, Phys. Rev. D **109**, 063024 (2024), arXiv:2311.04982 [astro-ph.HE].

[23] V. S. Paliya, A. Domínguez, M. Ajello, A. Franckowiak, and D. Hartmann, Fermi-LAT Stacking Analysis Technique: An Application to Extreme Blazars and Prospects for their CTA Detection, ApJ **882**, L3 (2019), arXiv:1908.02496 [astro-ph.HE].